# NQR Imaging *

Rainer Kimmich, Eberhard Rommel, and Peter Nickel
Sektion Kernresonanzspektroskopie, Universität Ulm, Ulm, FRG

Daniel Pusiol
FAMAF, Universidad Nacional de Córdoba, Córdoba, Argentina

Z. Naturforsch. **47a**, 361–366 (1992); received June 8, 1991

A rotating-frame NQR imaging ($\varrho$NQRI) procedure based on pure NQR is reported. The technique is suitable for powdery or crystalline solid materials containing quadrupole nuclei. The spatial information is encoded by gradients of the radio frequency amplitude of the excitation pulse. A special deconvolution procedure has been developed for the analysis of the spatial information encoded in the pseudo-FID of the NQR signal in the case of powder geometry. The technique is applicable to rotationally symmetric as well as to asymmetric electric field gradient tensors. The RF gradients are suitably produced by surface coils. The prominent advantage of surface-coil NQR is that objects larger than the coil diameter can be investigated. The imaging procedure then provides depth resolution in a range of the order of the coil radius. The technique is particularly suitable for the detection of gradients of physical parameters influencing the NQR line shift and of spatial distributions of the chemical composition. Examples are stress or temperature gradients. Two-dimensional images have been produced by rotating the sample step by step. For each orientation a profile across the sample is evaluated as the projection on the direction of the radio-frequency gradient. A projection-reconstruction formalism then permits the rendering of two-dimensional NQR images.

*Key words:* NQR, Imaging, Rotating-frame zeugmatography, Surface coil, Backprojection, Deconvolution.

## 1. Introduction

Spatially resolved nuclear quadrupole resonance (NQR) or even NQR imaging is a field which is of particular interest for the characterization of solid materials containing quadrupole nuclei. Two techniques connecting spatial information with NQR have been published in recent papers [1–3]. We are referring here to the rotating frame NQR imaging or $\varrho$NQRI techniques shown in Fig. 1 [2, 3] which are analogous to the rotating frame NMR zeugmatography technique in the amplitude encoding version [4]. The rotating frame method is particularly advantageous because one makes use of really pure NQR without any magnetic fields or magnetic field gradients. Thus the full spectroscopic information remains unconcealed and can be used for the characterization of the material.

With this technique the spatial information is amplitude-encoded in the free-induction decay (FID) signals by the aid of gradients $G_1$ of the local radio frequency (RF) amplitude $B_1$. This gradient vector may be aligned along the probe coil axis $z$, for instance

$$G_1(z) = \frac{\partial B_1(z)}{\partial z}. \tag{1}$$

In the course of an imaging experiment, the RF amplitude and/or the excitation pulse length is incremented step by step, so that finally a "pseudo-FID" is formed as a sequence of amplitudes of the proper FIDs or – after Fourier transformation of the FIDs – as a sequence of the intensities of a selected NQR line.

The excitation pulse is characterized by the effective pulse length

$$t_p = \alpha t_w \quad (0 \leq \alpha \leq 1). \tag{2}$$

$t_w$ is the proper pulse length, $\alpha$ the transmitter attenuation factor of the maximal RF amplitudes $B_1(z)$. In the experiments, $t_p$ is varied either by incrementing $t_w$ or $\alpha$ (compare Figure 1). In analogy to Fourier transform NMR we define the pseudo-dwell time $t_d$ and the pseudo-dwell amplitude $\alpha_d$, respectively. A pseudo-acquisition time $t_a$ and a pseudo-acquisition ampli-

* Presented at the XIth International Symposium on Nuclear Quadrupole Resonance Spectroscopy, London, U.K., July 15–19, 1991.

Reprint requests to Prof. Dr. Rainer Kimmich, Sektion Kernresonanzspektroskopie, Universität Ulm, Albert-Einstein-Allee 11, W-7900 Ulm, Germany.

0932-0784 / 92 / 0100-0361 $ 01.30/0. – Please order a reprint rather than making your own copy.

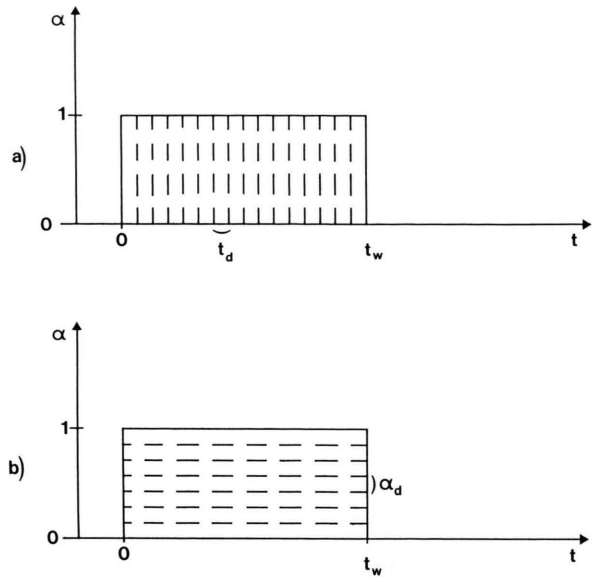


Fig. 1. $\varrho$NQRI RF pulse schemes. $\alpha$ is the pulse amplitude relative to its maximum value. $t_w$ is the pulse width. The pulses are incremented either by $t_d$, the pseudo-dwell time, or by $\alpha_d$, the pseudo-dwell amplitude. The RF amplitude varies linearly across the sample. Otherwise the results must be corrected [2]. (a) Variation of the pulse width. (b) Variation of the pulse amplitude.

tude $\alpha_a$ can be defined correspondingly for the two versions of the experiment. In the following we will consider the effective pulse length $t_p$ without any specification how the increment is performed.

With powder geometries one has to take into account the orientational distribution of the electric field gradient (EFG) tensor with respect to the RF coil axis [5]. The consequence is a flip angle distribution which affects the evaluation of the amplitude-encoded signal. As pointed out in [3], the standard Fourier transform analysis [6] used for the evaluation of pseudo-FIDs provides correct spatial profiles for single crystals. There are, however, distortions in the more practical case of powder geometries. Therefore a numerical deconvolution procedure has been developed which produces the true profiles even with powder distributions of the electric field gradient orientations.

Two- (or three-) dimensional images can be rendered by recording a series of profiles in different directions across the sample and using the backprojection procedure [7]. Profiles in varying directions can be recorded by changing the direction of the RF gradient relative to the sample. In principle this can be done by the appropriate superposition of the RF fields of an orthogonal coil system or simply by mechanical rotation of the sample step by step in the RF gradient of a single coil. In this study the latter method was applied.

## 2. Deconvolution Analysis

A certain NQR line of spin-$\frac{3}{2}$-nuclei is considered. The angular frequency be $\omega = \omega_0$. The local lineshape is represented by $g(\omega, z)$. The pseudo-FID of materials with powder geometry is then given by [8, 9]

$$S(t_p) = c \int_0^\infty dz\, \tilde{\varrho}(z) \frac{1}{\pi} \int_0^\pi d\theta \frac{1}{2\pi} \int_0^{2\pi} d\phi\, r(\theta, \phi) \sin\theta \cdot \sin \frac{\sqrt{3}\, t_p\, \omega_1(z)\, r(\theta, \phi)}{2(1+\frac{1}{3}\eta^2)^{1/2}} \quad (3)$$

with

$$\tilde{\varrho}(z) = g(\omega, z)\, \varrho(z), \quad (4)$$

$$\omega_1(z) = \gamma B_1(z), \quad (5)$$

$$r(\theta, \phi) = [4\eta^2 \cos^2\theta + (9 + \eta^2 + 6\eta \cos 2\phi) \sin^2\theta]^{1/2}. \quad (6)$$

$\tilde{\varrho}(z)$ is the proper distribution, $\varrho(z)$, of the number density of nuclei resonant at $\omega_0$ weighted by the lineshape function $g(\omega)$, $c$ is a numerical factor. This is the profile of the sample to be determined. Other quantities in the above expressions are: $\theta$ and $\phi$, the polar and azimuthal angles of the electric field-gradient principal axis with respect to the laboratory frame axis $z$ which is virtually identical to the coil axis; $\hbar$, Planck's constant; $\gamma$, gyromagnetic ratio.

With this expression for the FID we have assumed that the spatial resolution of the technique is beyond the orientational correlation length of the powder, of course. In principle, the integrand in the above formula should be supplemented by a factor taking into account the relaxation decay during $t_w$. We omit it here for simplicity.

In the axially symmetric case ($\eta = 0$), the above formula simplifies to [5]

$$S(t_p) = 3c \int_0^\infty dz\, \tilde{\varrho}(z) \frac{1}{\pi} \int_0^\pi d\theta \sin^2\theta \cdot \sin[\sqrt{3}\, t_p \sin\theta\, \omega_1(z)/2]. \quad (7)$$

For constant RF field gradients, $G_1(z) = \text{const}$, we have

$$\omega_1(z) = \gamma G_1 z. \quad (8)$$

In analogy to the NMR case, a "$k$ space" [7] component

$$k = \sqrt{3}\gamma G_1 t_p/2 \tag{9}$$

may be defined.

The above expressions for the pseudo-FIDs can be written as

$$S(t_p) = c \int_0^\infty \mathrm{d}z\, \tilde{\varrho}(z) f(z t_p) \tag{10}$$

with

$$f(z t_p) = \frac{1}{\pi} \int_0^\pi \mathrm{d}\theta \frac{1}{2\pi} \int_0^{2\pi} \mathrm{d}\phi\, r(\theta, \phi) \sin\theta \cdot \sin \frac{\sqrt{3}\, t_p\, \omega_1(z)\, r(\theta, \phi)}{2(1+\frac{1}{3}\eta^2)^{1/2}} \tag{11}$$

The substitution

$$t_p = t_d\, e^u, \quad z = z_0 e^{-v} \tag{12), (13}$$

leads to

$$S(t_p) = c \int_{-\infty}^\infty \mathrm{d}v\, z_0\, \tilde{\varrho}(z_0) f(z_0\, t_d\, e^u), \tag{14}$$

i.e. to the convolution expression (compare [10])

$$\tilde{S}(u) \equiv S(t_d\, e^u) = c \int_{-\infty}^\infty \mathrm{d}v\, f_a(v)\, f_b(u-v), \tag{15}$$

where

$$f_a(v) = z_0\, e^{-v}\, \tilde{\varrho}(z_0 e^{-v}), \tag{16}$$

$$f_b(\zeta) = f(z_0\, t_d\, e^\zeta) = \frac{1}{\pi} \int_0^\pi \mathrm{d}\theta \frac{1}{2\pi} \int_0^{2\pi} \mathrm{d}\phi\, r(\theta, \phi) \sin\theta \cdot \sin \frac{\sqrt{3}\, r(\theta, \phi)\, \gamma\, G_1\, z_0\, e^{-v}\, t_d\, e^\zeta}{2(1+\frac{1}{3}\eta^2)^{1/2}} \tag{17}$$

with $\zeta = u - v$. Note that the above substitution corresponds to a transformation from linear scales $(t_p, z)$ to logarithmic scales $(u, v)$.

Deconvolution is performed by the aid of the convolution theorem, i.e.

$$f_a(v) = \mathscr{F}_u^{-1} \left\{ \frac{\mathscr{F}_u\{S(t_d\, e^u)\}}{\mathscr{F}_\zeta\{f_b(\zeta)\}} \right\}. \tag{18}$$

$\mathscr{F}_\xi$ and $\mathscr{F}_\xi^{-1}$ denote the Fourier transform operator and the inverse Fourier transform operator, respectively, where the forward Fourier transform refers to a variable $\xi$.

$S(t_d\, e^u)$ represents the data set derived from the experiments. $f_b(\zeta)$ is a known function given by the above expressions. $f_a(v)$ thus can be derived numerically. The desired profile of the sample finally is given by the relation

$$\tilde{\varrho}(z) = \frac{f_a(v)}{z}, \tag{19}$$

where

$$v = \ln \frac{z_0}{z}. \tag{20}$$

The evaluation procedure was tested by the aid of the profile given in Figure 2a. Figure 2b shows the corresponding pseudo-FID calculated by (7) assuming an asymmetry parameter of $\eta = 0$. Figure 2c shows the pseudo-FID in the logarithmic scale.

The data set representing the convolution function $f_b(\zeta)$ was calculated by carrying out the integrals in (17) numerically by a simple summing-up procedure. 256 oscillations of this function were taken into account. The result is shown in Figure 2d. The Fourier transforms were obtained by the standard FFT method [11].

Figure 2e shows the reconstructed profile. The result shows that the original profile is well reproduced provided a sufficiently high number of data points is used in the logarithmic scale.

The proposed algorithm needs more memory and computer processing time than the simple Fourier transform analysis used in our previous studies [2, 3]. On the other hand, a much better reconstruction quality is guaranteed for powder geometries, and the reproduced profiles do not tend to be smeared out.

## 3. ϱNQRI Experiments

The main features of the transmitter/receiver electronics and the control computer system of the home-built NQR spectrometer used in this study have been described elsewhere [2, 3]. For this apparatus a new 2D imaging probehead was constructed. A scheme is shown in Figure 3. The probehead consists of a four-turn surface coil, a sample holder which can be revolved by the aid of a stepping motor. The motor is controlled by a pulse programmer board (SMIS PP 2000) installed in the system computer (HP Vectra RS/25C). The surface coil serves as transmitter and as receiver coil as well.

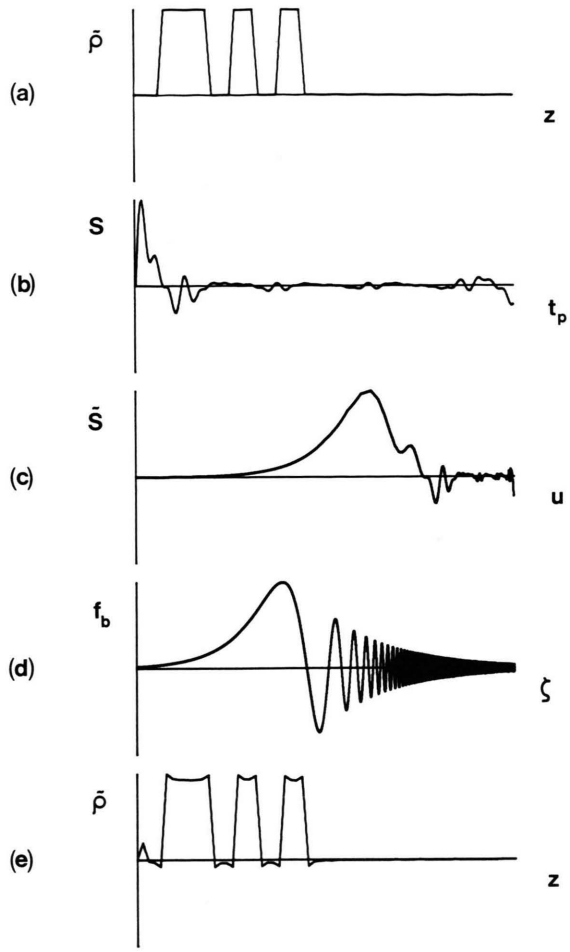


Fig. 2. (a) Profile used for tests of the reconstruction algorithm. Numerically the profile was represented by 64 data points distributed equally in the shown range of $z$ with arbitrary units. (b) Pseudo-FID of the test profile shown in (a). 256 data points were calculated on the basis of (7). This representation refers to a linear scale of the $t_p$ axis. (c) Pseudo-FID of (b) represented on the logarithmic scale. 8192 data points were calculated by the aid of the linear interpolation of the data on which the representation on the linear scale is based. The data points are distributed equally along the $u$ axis. (d) Convolution function $f_b(\zeta)$ on a logarithmic scale. The number of data points is 8192 again. (e) Profile reconstructed by the aid of the deconvolution algorithm. The range of the $z$ axis is the same as in (a).

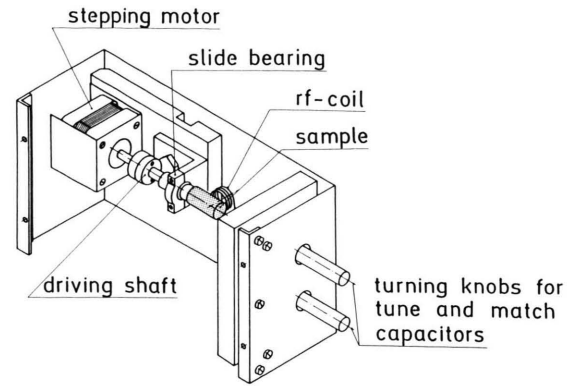


Fig. 3. Sample revolution probehead for two-dimensional $\varrho$NQRI. The diameter of the four-turn surface coil was 16 mm.

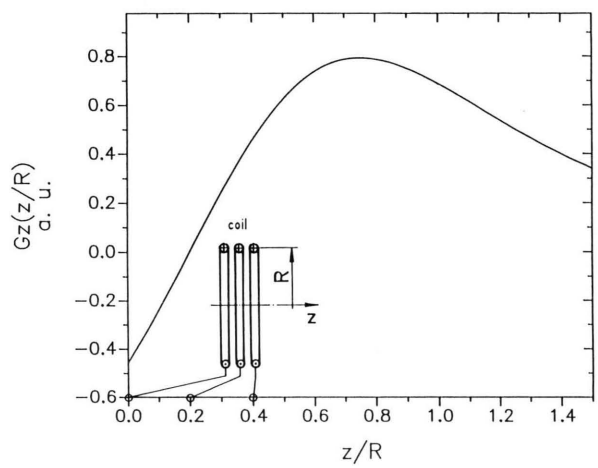


Fig. 4. Calculated gradient of the RF amplitudes (arbitrary units) along the axis of a three-turn surface coil. Note that the gradient of the RF amplitude does not vary strongly in the range which is typically used for the studies proposed in this paper.

The diameter of the surface coil was 16 mm, the length 6 mm. The coil was tuned to 116.22 MHz, i.e. to the NQR resonance frequency of arsenic in arsenolite ($As_2O_3$) which was used as test substance. The coil axis is perpendicular to the sample rotation axis. The RF gradient produced by the surface coil geometry does not vary very strongly in the sample range. A typical distance dependence of the RF gradient calculated for a three-turn surface coil is shown in Figure 4. Therefore the evaluation of the pseudo-FIDs was carried out under the assumption of constant gradients of the RF amplitude. In cases where this should be not precise enough, a post-detection correction by rescaling of the $z$ axis compensating the actual $z$ dependence of the RF gradient is easily possible [1].

A schematic cross section of the test sample is shown in Figure 5a. The sample consisted of polymethylmethacrylate (PMMA) cylinders (diameter 12 mm, length 23 mm) with holes having circular cross sections. The long axis of the holes was parallel to the cylinder axis coinciding with the revolution axis. The holes were filled with arsenolite powder.

(a)

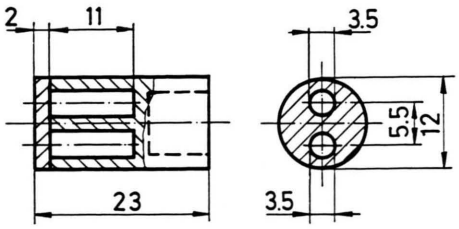


(b)


Fig. 5. Cross sections (a) of the test sample investigated and NQR image counterpart (b) recorded as described in the text. The sample consisted of a PMMA cylinder with bores filled with arsenolite ($As_2O_3$) powder. The contrasts represent the spatial distribution of the arsenic nuclei. The dimensions indicated in the scheme are given in millimeters.

FID-signals were recorded with varying lengths of the RF pulse. The RF pulse length was incremented in steps of 3 μs ($\alpha = 1$ so that $t_p = t_w$). 64 single-scan experiments were carried out for each sample orientation. The maximum signal amplitude was found for $t_w = 6$ μs.

Each FID was Fourier transformed. From the data set of 116.22 MHz resonance line a pseudo-FID was formed where the time axis refers to the pulse length.

The pseudo-FIDs were phase and baseline corrected. After erasing the imaginary part, the pseudo-FIDs were multiplied by the filter function [12]

$$f(x) = \tfrac{1}{2}\, x(1 - \cos x), \tag{21}$$

where

$$x = \pi \frac{t_w}{t_a} \tag{22}$$

($t_a$ is the pseudo-acquisition time). The pseudo-FIDs were analyzed following the procedure described above assuming $\eta = 0$.

The sample was revolved step by step so that profiles across the sample in different directions were obtained. Pseudo-FIDs for 50 sample orientations were recorded. The increment step of the sample revolution was 3.6° so that the sample was turned in total by 180°. The measurement of the 50 projection profiles took about 45 minutes, where the limiting factor was the time needed for writing the pseudo-FID data on the hard disk. (The room-temperature spin-lattice relaxation time of arsenolite is comparatively short: $T_1 \approx 10 \ldots 100$ ms [13].)

Finally the profiles recorded for the different sample orientations had to be centered with respect to the revolving axis. This was done by bringing the extension of profile pairs recorded with orientation angle differences of 180° into coincidence.

Signals recorded in different distances from the center of the surface coil in principle contribute differently to the signal and are weighted by a corresponding weighting function. As long as constant RF gradients are applied, the distance weighting is compensated in the final backprojection procedure, because profiles of the sample turned by angles in the full range of 180° are superimposed. Therefore corrections of this kind were omitted.

From the profile data sets, 2D images were reconstructed using the backprojection method which was already applied by Lauterbur in his first imaging paper [14]. An exemplary result is shown in Figure 5b. The geometry of the sample (Fig. 5a) is clearly rendered. Thus the feasibility of the technique has been demonstrated.

## 4. Conclusions and Discussion

The ϱNQRI method in combination with a surface coil/sample revolution probehead permits the record of 2D images of the distribution of compounds with quadrupole nuclei. The image contrasts may be weighted by other factors such as relaxation times or the linewidth. The full spectroscopic information is maintained because no readout field gradient is used. Therefore selective images based on certain resonance lines can be recorded. The technique is applicable to single crystals as well as to samples with powdery geometry. For the latter case a special deconvolution signal processing algorithm has been developed ensuring that the true sample profiles are rendered.

A drawback of NQR imaging is that the experimental setup must be adapted not only to a certain quadrupole nucleus but also to a certain compound.

Therefore it should more precisely be designated as an "NQR compound" imaging. On the other hand, having chosen a suitable compound, one can use this substance as a probe for material properties. In this sense the high susceptibility of NQR lines to structural parameters, stress and temperature suggests to use the technique for rendering images of just these quantities. In a previous article [2] we have shown that the temperature induced line shifts can be calibrated to the temperature, so that temperature gradients can be imaged. The same should be feasible with stress. Perspectives on this basis are solutions of practical problems in material science and process engineering.

*Acknowledgements*

Thanks are due to B. Fundel and J. Wiringer who assisted in the course of this work. Financial support from the Deutsche Forschungsgemeinschaft, the Deutscher Akademischer Austauschdienst, and the Alexander von Humboldt foundation is gratefully acknowledged.

[1] S. Matsui, K. Kose, and T. Inouye, J. Magn. Reson. **88,** 186 (1990).
[2] E. Rommel, P. Nickel, R. Kimmich, and D. Pusiol, J. Magn. Reson. **91,** 630 (1991).
[3] E. Rommel, D. Pusiol, P. Nickel, and R. Kimmich, Measurement Sci. Technology **2,** 866 (1991).
[4] D. I. Hoult, J. Magn. Reson. **33,** 183 (1979).
[5] M. Bloom, E. L. Hahn, and B. Herzog, Phys. Rev. **97,** 1699 (1955).
[6] R. R. Ernst and W. A. Anderson, Rev. Sci. Instrum. **37,** 93 (1966).
[7] P. Mansfield and P. G. Morris, NMR Imaging in Biomedicine, Academic Press, New York 1982.
[8] J. C. Pratt, P. Raghunathan, and C. A. McDowell, J. Magn. Reson. **20,** 313 (1975).
[9] G. S. Harbison, S. Slokenbergs, and T. M. Barbara, J. Chem. Phys. **90,** 5292 (1989).
[10] R. Bisseling and R. Kosloff, J. Comp. Physics **59,** 136 (1985).
[11] J. W. Cooley and J. W. Tukey, Math. Comput. **19,** 297 (1965).
[12] C.-M. Lai, J. Appl. Phys. **52,** 1141 (1981).
[13] D. J. Treacy and P. C. Taylor, Solid State Comm. **40,** 135 (1981).
[14] P. C. Lauterbur, Nature London **242,** 190 (1973).